Accepted Manuscript

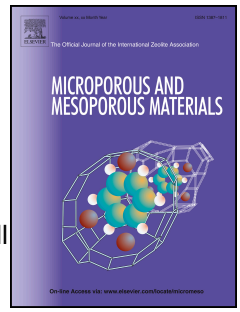

Porous carbons from inverse vulcanized polymers

Joseph C. Bear, James D. McGettrick, Ivan P. Parkin, Charles W. Dunnill, Tom Hasell

PII: S1387-1811(16)30216-5

DOI: 10.1016/j.micromeso.2016.06.021

Reference: MICMAT 7763

To appear in: *Microporous and Mesoporous Materials*

Received Date: 26 February 2016

Revised Date: 27 May 2016

Accepted Date: 12 June 2016

Please cite this article as: J.C. Bear, J.D. McGettrick, I.P. Parkin, C.W. Dunnill, T. Hasell, Porous carbons from inverse vulcanized polymers, *Microporous and Mesoporous Materials* (2016), doi: 10.1016/j.micromeso.2016.06.021.

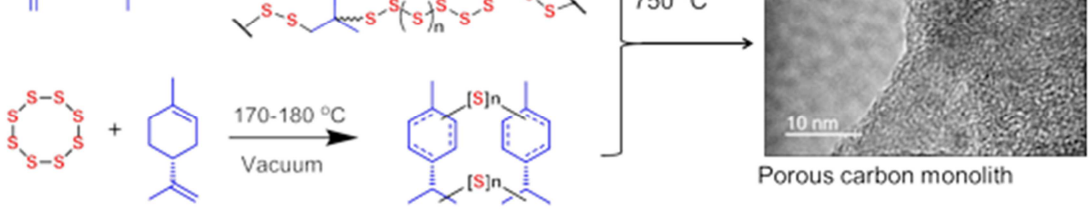

Porous carbon monolith

and Tom Hasell[4]*

[1] Energy Safety Research Institute (ESRI), College of Engineering, Swansea University, Bay Campus, Fabian Way Swansea, SA1 8EN, UK. E-mail: c.dunnill@swansea.ac.uk

[2] SPECIFIC, College of Engineering, Swansea University, Bay Campus, Swansea, SA1 8EN, UK.

[3] Department of Chemistry, University College London 20 Gordon Street, London, WC1H 0AJ, UK

[4] Department of Chemistry, University of Liverpool, Crown Street, Liverpool, L69 7ZD, UK. E-mail: t.hasell@liverpool.ac.uk

Abstract:

Elemental sulfur is an underutilised industrial by-product. It has been recently shown that it can be simply and scalably co-polymerised, by "inverse vulcanisation" with organic crosslinkers. The properties of porous carbons, which have extensive uses in science and industry, are influenced by the materials from which they are generated. Reported here are the first examples of porous carbons produced from high-sulfur inverse vulcanised polymers. The materials produced show micro-porosity, gas selectivity, and are doped with sulfur. The simplicity of the technique, and wide range of other potential inverse vulcanised feedstocks, gives scope for transferability and control of properties.

Keywords: Inverse vulcanisation, sulfur, porous carbon, gas separation, microporous

interact with atoms, ions and molecules throughout the bulk of the material.[1] This has led to widespread uses in adsorption, catalysis, separation, purification, and energy storage and production.[2] Activated carbon is perhaps the original and most highly used adsorbent material, simply generated from the pyrolysis of any number of carbonaceous starting materials (coal, wood, coconut husks etc).[3] Activated carbon is produced in vast quantities annually and used in bulk worldwide not only for gas storage and separation,[4] but also filtering organic[5, 6] and inorganic[7] toxic pollutants from drinking water, and for electrode and super-capacitor applications.[8, 9] While bio-waste provides an ideal feedstock for activated carbons in terms of low cost and availability,[6, 10] this can mean the internal surfaces of activated carbons are often quite poorly defined in terms of chemical functionality, reproducibility, and pore size.[3] Recently, there has been interest in producing porous carbons from feedstock materials with more defined structures, such as carbides,[11, 12] coordination-polymers,[13] synthetic organic polymers[14, 15] and hyper-crosslinked polymers,[16] in order to control the resultant chemical functionality, pore distribution, and reproducibility with more precision. Here we show for the first time that "inverse-vulcanised" polymers can be used as templates to produce porous carbons with narrow pore-size distributions.

Sustainable chemical processes and those using waste materials provide alternate routes to a more environmentally benign economy of chemical utilisation. Sulfur is a promising alternative feedstock to carbon for polymeric materials and is a by-product from hydrodesulfurisation; a crucial step in the petroleum refining process.[17] This has led to vast unwanted stockpiles of sulfur, as supply greatly exceeds demand,

opening polymerisation (ROP) to form polymeric sulfur of high molecular weight. However, this form is not stable, and it readily depolymerises back to the monomeric S_8 rings. It has been recently shown that 'inverse vulcanisation' can be used to stabilise sulfur in its polymeric form.[18-20] In conventional vulcanisation, polydienes are crosslinked by a small fraction of sulfur to form synthetic rubber. In inverse vulcanisation, polymeric sulfur is stabilised against depolymerisation by copolymerisation of a large amount of sulfur with a modest amount of small molecule dienes. The term "inverse vulcanisation" was first coined by Pyun *et al*[18] in 2013, when they reported high sulfur polymers crosslinked with 1,3-diisopropenyl benzene (DIB), (Scheme. 1a). These S-DIB copolymers were then foamed in supercritical carbon dioxide by Hasell *et al.* to produce macroporous solids which were shown to be effective for mercury capture from water.[21] Similarly, Chalker *et al.* were able to demonstrate a limonene based inverse vulcanised polymer for potential applications in mercury remediation.[22] (Scheme. 1b). Sulfur is produced annually in excess of 60 million tons and more than 70 thousand tons of limonene are isolated each year from orange zest in the citrus industry.[22] The resultant sulfur-limonene polysulfide is therefore inexpensive, and a suitable source for porous carbon materials, as may be many of the wide range of other inverse vulcanised polymers,[18, 22-28] either those reported so far, or those likely to be reported in the next few years, especially those from renewable sources. We found that the properties of the porous materials produced by a simple carbonisation process (Scheme 1c), such as surface area or effective gas

Experimental

Materials: Sulfur (≥99.5 %), poly(4-styrenesulphonate) (average M_w ~ 70000, powder), and limonene (>93%) were purchased from Sigma Aldrich and used as received. 1,3-diisopropenylbenzene (>97 %) was purchased from TCI and used as received.

Synthesis of sulfur-1,3-diisopropenyl benzene (S-DIB) copolymer:

The sulfur polymer was synthesised according to the protocol developed by Chung *et al.*[18] with modifications. The following protocol is for 50 wt. % DIB polymer: Briefly, elemental sulfur (S_8, 2g, 7.81 mmol) was added to a vial and heated to 185 °C in an oil bath under vigorous stirring. Once 185 °C was reached, DIB (2.16 mL, 12.6 mmol) was injected, the whole mixture agitated with a glass rod and stirred for 4-5 minutes. Calculations for different DIB:S polymer compositions are given in table 1. At this point, the solution was poured into a mould and cured for 30 minutes in a pre-heated 200 °C oven.

After 30 minutes, the mould was removed and the polymer allowed to cool to room temperature in air. The polymer samples were then ground to a coarse powder using a pestle and mortar. Due to the low glass transition temperature of the sulfur-DIB polymers, it was helpful to place the bulk polymer in the freezer prior to grinding. The coarse granules were then placed evenly into a long ceramic crucible and placed into a tube furnace. Nitrogen gas was passed over the sample for 30 minutes at a flow rate of

maintained at 600 cm^3/min throughout.

S-limonene synthesis: Closely following the procedure previously reported:[22] Sulfur (25.0 g, 97.5 mmol, S_8) was added to a 100 mL round bottom flask equipped with a stirrer bar. The flask was then placed in an oil bath pre-heated to 170 ºC and stirred vigorously. After 30 minutes, limonene (25.0 g, 29.6 mL, 183 mmol) was added carefully over 2 to 5 minutes. The flask was then equipped with distillation head and condenser. After another 60 minutes the temperature was increased 180 ºC and volatile material was removed by vacuum distillation (~50 mm Hg). The non-volatile material remaining in the flask was then cooled and dried further under high vacuum (< 1 mm Hg) at 100 ºC overnight. After cooling to room temperature, the final product vitrified and was obtained as a dark red material. ^{1}H NMR is in agreement with previously published results (Fig. S1).[22]

Carbonisation method:

Carbonisation of the sulfur polymer was achieved by annealing ~ 4 g of the chosen sulfur polymer at 750 °C. The sulfur polymer was ground before loading into a ceramic trough. If the polymer became sticky with grinding, it was frozen (-20 °C) to increase brittleness. The polymer was then loaded into a tube furnace and subjected to nitrogen flow for 1 hour (600 sccm) before heating to 750 °C at a heating rate of 10 °C min^{-1}, maintaining 750 °C for 1 hour. When the temperature reached 350 – 400 °C, it is noteworthy that elemental sulfur leaches out of the structure and exits the furnace via

Instrumentation:

Gas Sorption Analysis: Surface areas were measured by nitrogen adsorption and desorption at 77.3 K. Powder samples were degassed offline at 100 °C for 15 h under dynamic vacuum (10-5 bar) before analysis, followed by degassing on the analysis port under vacuum, also at 100 °C. Isotherms were measured using Micromeritics 2020, or 2050 volumetric adsorption analyzer.

X-Ray photoelectron (XPS) spectroscopy: XPS spectra were recorded on a K-alpha instrument (Thermo Fisher Scientific, East Grinstead, UK) using a monochromated Al Kα source. All spectra were recorded using a charge neutralizer to limit differential charging and subsequently calibrated to the main adventitious CxHy carbon peak at a binding energy of 284.8 eV. Survey scans were recorded at a pass energy of 200 eV and step size of 1 eV. High resolution scans of S (2p), C (1s) and O (1s) were recorded at a pass energy of 50 eV with 0.1 eV step size. Data was fitted using CASA XPS with Shirley backgrounds.

Electron microscopy: Transmission electron microscope (TEM) images were obtained using a high resolution TEM Jeol 2100 with a LaB_6 source operating at an acceleration voltage of 200 kV. Images were recorded on a Gatan Orius Charge-coupled device (CCD). Samples were prepared by drop-casting a sonicated suspension of the annealed S-polymer powders in n-hexane onto a copper 400 mesh TEM grid with a holey carbon film (Agar Scientific Ltd.). Energy dispersive X-Ray spectra (EDS) were recorded on an

voltage of 15 kV.

Results

Sulfur polymers were synthesised *via* "inverse vulcanisation" polymerisation, involving the addition of an aromatic, divinylic cross-linker (1,3-diisopropenylbenzene or limonene) to molten elemental sulfur. This reaction forms a red, intractable solid which was then annealed under a flow of nitrogen at 750 °C yielding a highly porous, sulfur-carbon framework. Several S-polymers with differing wt. % ratios of sulfur to 1,3-diisopropenylbenzene were examined.

During the annealing process, it was observed that elemental sulfur leached out of the structure due to large quantities of yellow powder appearing in the tube furnace exhaust. The exhaust tube was run through water, into which particulate sulfur precipitated, and was confirmed to be α-sulfur by PXRD (Fig. S2). H_2S and CS_2 gas were also detected in the exhaust stream by mass (predominant [M+] at 34 and 76 respectively). The production of H_2S was further confirmed by placing lead(II) acetate trihydrate and copper(II) chloride dehydrate in the gas stream, both of which turned black indicating the presence of H_2S over SO_2. The sulfur leaching process ceased as the temperature increased beyond ~650 °C, presumably as all sulfur not intrinsic to the structure had exited. Capture and re-use of leached sulfur from this process would therefore be industrially viable if required on scale-up.

On cooling, all products were a shiny-metallic grey black in colour, and despite being ground and placed as a powder in ceramic bricks before entering the furnace, the

large, unbroken monolith (figure S6, graphical abstract). 20 g of obtained product was an arbitrary quantity, so the process could potentially be scaled-up.

The effect the inverse vulcanisation polymers had on the resultant structures was examined using poly(4-styrenesulphonate) (a sulfur containing polymer) as a control to see if the inverse vulcanisation was important or merely the mixing in with sulfur before carbonisation. Traditional “activators” such as potassium hydroxide for activated carbon based porous structures were also used, leading to no porosity or sulfur leaching and a solid mass present in the base of the ceramic trough.

SEM imaging of the samples reveals relatively coherent and smooth surfaces when a lower percentage of sulfur is used, but a granular structure of micro-spheres when a higher percentage of sulfur is used (Figure 1). This is likely the result of the removal of sulfur during the carbonisation – lower sulfur inclusion allowing retention of original shape, but higher sulfur inclusion causing a contraction on removal, leading to the formation of agglomerated sub-micron spheres. It is noteworthy that in the intermediate samples (*i.e.* 30 and 40 wt. % DIB) there is evidence for both morphologies, indicating that the resultant structure can be directly related to the amount of sulfur:DIB in the original polymer.

Closer investigation of the higher DIB content materials, by TEM, reveals the internal structure of these materials (Figure 2). This perhaps gives some understanding of why the larger monolithic structure, and smooth surface are maintained. While the loss of sulfur results in the formation of internal voids, the material left effectively forms struts, maintaining a coherent structure. There is also evidence of crystallinity in

EDS analysis of the TEM samples (Figure 2 d)) indicated the presence of sulfur and carbon with copper (a consequence of the copper TEM grid), chromium and iron (from the steel TEM goniometer), silicon (used as a lubricant in the manufacture of glass vials, from the original polymer synthesis) and oxygen (present from the combustion process). EDS analysis showed that the sulfur to carbon ratio in the structure was 87.9 C to 12.1 S (in at. %, 40 wt. % DIB sample), showing the decrease in sulfur attributed to the leaching out in the annealing process. The TEM grids themselves contain a carbon film, causing a slight overestimation of the carbon content.

The EDS analysis was supported using quantitative XPS. XPS showed that the ratio of carbon : sulfur didn't alter significantly after annealing despite large variations in carbon:sulfur content in the starting materials. The results are summarised with the initial composition of samples in Table 1. In all samples, there appears to be between 7.4 and 14.1 % sulfur composition when compared to carbon (assuming the structures are composed entirely of carbon and sulfur). This suggests there is a critical amount of sulfur which remains in the structure, no matter how high the initial concentration, leading to the frameworks seen by electron microscopy in Figures 1 and 2. It is likely that a higher initial concentration of sulfur leads to longer polysulfide chains (S-S_n-S) between the –C-S- linkages. As S-S bonds are reversible, especially at elevated temperatures, this leads to a loss of these extended groups as the material forms shorter, e.g. mono- or di-sulfide, linkages, which are more stable and account for the remaining sulfur content.

samples are mostly comprised of sulfur and carbon, and high resolution scans of those environments elucidated details about the surface chemistry. High resolution S(2p) analysis revealed a highly complex spectrum with two distinct sulfur chemical environments, the first doublet with its S $2p_{3/2}$ peak at 168.0 eV is ascribed to organic sulfate groups – as expected this signal is more pronounced for systems where larger O(1s) peaks are observed. A second, stronger doublet is observed with the S $2p_{3/2}$ peak at 164.0 eV, which accounted for *ca.* 80 % of the sulfur signal and ca. 8 % of the entire surface region. Several assignments are possible for this, but it is consistent with species such as thioethers or disulfides,[30, 31] showing the retention of sulfur despite the significant leaching observed during the annealing process.

Analysis of the C(1s) envelope shows a main peak assigned to 284.8 eV for hydrocarbons (*ca.* 65 at. % of total surface), which assumes that the bulk of the carbon aromaticity is lost in the carburization process, with low level peaks observed also for RCOOR environments at 288.7 eV and RCOR environments at 286.5 eV (comprising *ca.* 10 at. % of total surface). It is highly likely that surface oxide groups will be present, with similar results obtained for typical XPS analysis of carbonaceous materials such as carbon nanotubes.[27]

High resolution scans of the S2p regime revealed a highly complex environment, with regimes attributed to (S2p $_{3/2}$ binding energies quoted): C-S (163.98 eV) and sulfates (SO_x and R-SO_x-R′ 167.88 eV).[31] Regions at lower binding energy such as 161.5 eV were attributed as C=S, but were low intensity. The C-S 2p 3/2 and 2p ½ regions were the most intense, accounting for *ca.* 80 % of the sulfur signal and an

the retention of sulfur despite the significant leaching observed in the annealing process.

Gas sorption analysis shows microporosity is present in all of the carbonised S-DIB samples (Figure 4). In order to determine if the inverse vulcanisation (i.e. crosslinking of the polymeric sulfur by the organic phase) was important, we ran a control sample of Poly(4-styrenesulfonate) mixed with sulfur, without vulcanisation. This showed no porosity to nitrogen. However, the carbonised sulfur-limonene copolymer also showed no porosity to nitrogen. For the carbonised S-DIB samples it can be seen that the nitrogen uptake increases initially with DIB uptake (between 5 and 10 wt.% DIB) before becoming relatively consistent across the range of compositions (Fig. S3). The 5 wt.% DIB sample has an apparent Brunauer–Emmett–Teller surface area (SA_{BET}) of 223 $m^2 g^{-1}$. All of the samples with a higher % DIB component were >500 $m^2 g^{-1}$ (533, 537, 512, and 503 $m^2 g^{-1}$ for 10, 20, 40, and 50 wt. % respectively). It is possible that at the lowest % DIB component an insufficiently connected carbon-carbon bonded network is created, such that the structure collapses to an extent on removal of the sulfur. For the lower % DIB compositions (5-20 wt. %), some degree of meso-porosity is also detected, as indicated by the slope of the isotherm (Figure 4), and differential pore size distribution (Figure 5). This is consistent with the electron microscopy results, which showed aggregated sub-micron particles in these lower DIB proportion samples. It is likely that this mesoporosity results from the relatively high volume of sulfur removed during carbonisation – the sulfur effectively acting as a template. For the higher proportion DIB samples, for which the electron microscopy showed they were able to maintain a coherent macroscopic structure, no such meso-

higher proportion DIB samples show a remarkably narrow and defined range of pore sizes, for what is in essence an activated carbon, with the entire pore width range <2 nm. These samples also show significant CO_2 uptake, with the 10 wt.% DIB sample taking up over 15 wt.% CO_2 at 263 K (Fig. S4). The heat of adsorption of CO_2 onto these carbonised polymers is quite high, 29 kJ/mol (Fig. S5), in comparison to many common activated carbons, e.g. heats of adsorption of CO_2 in activated carbons Maxsorb III and ACF (A-20) are found to be (20.37 and 19.23) kJ/mol respectively.[32]

The S-Lim copolymer is known to form a lower molecular weight species in comparison to S-DIB, more a polysulfide than an extended, highly crosslinked polymer.[18, 22] Therefore was thought possible that the structure might be more able to 'close-up' during carbonisation, resulting in much narrower pores, and explaining the lack of porosity to nitrogen (Figure 4). In order to test this, the carbonised S-Lim was examined for uptake of smaller gasses, carbon dioxide and hydrogen (Figure 6). This revealed that although nitrogen is effectively shut off, the structure remains porous to carbon dioxide and hydrogen. This gives potential for gas separation applications, especially when combined with the possibility to melt process the pre-carbonised polymer into films/membranes. The molar selectivity to CO_2/N_2 at 273 K is 24 at 0.1 bar and 8 at 1 bar. The molar selectivity to H_2/N_2 at 77.3 K is 975 at 0.1 bar and 66 at 1 bar.

Discussion/conclusions

cost precursors (e.g. sulfur and limonene), and it is a simple one step process, with high atom efficiency and no exogeneous solvents or reagents. The carbonisation route itself is simple, scalable, allows for the reclaimation and re-use of the sulfur, and could be easily adapted to produce different architectures. The molten state formed by the S-polymer feedstock (100 °C for S-Lim, 200 °C for S-DIB), could be used to generate films, membranes, or coherent monoliths. The use of such porous carbon monoliths can be preferential to granular systems for applications from sorption[33, 34] to supercapacitance.[35] Porous membranes are routinely widely used industrially for both gas and liquid phase separations.[36-39] The resultant materials are left doped with small amounts of sulfur. This could have interesting effects in both electrochemistry[40-42] and sorption[42-46] applications, as sulfur doping has been used in both of these fields to enhance properties and function. Disulfide linked polymer networks have been shown to demonstrate effective separation of organics from water.[47]

The porous carbons produced show a microporosity with well defined pore distribution (S-DIB) or the potential for gas selectivity (S-Lim). This gives potential for separation of gas mixtures that are of industrial relevance, such as CO_2/N_2[48] for application post-combustion CO_2 capture, and H_2/N_2[49]. The properties of the porous carbons produced was found to depend on both the S:organic ratio used, and the nature of the organic crosslinker. Given the wide range of possible inverse vulcanisation crosslinkers, and the scope to mix multicomponent systems, this gives a remarkable potential for control and tenability.

materials, with properties dependent on sulfur ratio and crosslinker choice. The retention of sulfur in the microporous carbon structure, with implications in widespread applications, and scope for variation in structure suggest many more such materials could be reported in the future.

Acknowledgements

We thank Rob Clowes for assistance with gas sorption measurements. T.H. is a Royal Society University Research Fellow. CWD and JCB thank the Ramsay Memorial Trust for past and present Ramsay Fellowships. We thank Dr Michael J. Powell (UCL) for his help with the exhaust gas analysis and Dr Kersti Karu for mass spectroscopy analysis as part of the UCL Mass spectroscopy service.

References

1. M. E. Davis, *Nature*, 2002, **417**, 813-821.
2. A. G. Slater and A. I. Cooper, *Science*, 2015, **348**, 985-988.
3. R. E. Morris and P. S. Wheatley, *Angewandte Chemie-International Edition*, 2008, **47**, 4966-4981.
4. S. Sircar, T. C. Golden and M. B. Rao, *Carbon*, 1996, **34**, 1-12.
5. A. Dabrowski, P. Podkoscielny, Z. Hubicki and M. Barczak, *Chemosphere*, 2005, **58**, 1049-1070.
6. C. Namasivayam and D. Kavitha, *Dyes and Pigments*, 2002, **54**, 47-58.
7. D. Mohan and K. P. Singh, *Water Research*, 2002, **36**, 2304-2318.
8. E. Frackowiak and F. Beguin, *Carbon*, 2001, **39**, 937-950.
9. V. Ruiz, C. Blanco, R. Santamaría, J. M. Ramos-Fernández, M. Martínez-Escandell, A. Sepúlveda-Escribano and F. Rodríguez-Reinoso, *Carbon*, 2009, **47**, 195-200.
10. A. Ahmadpour and D. D. Do, *Carbon*, 1997, **35**, 1723-1732.
11. Y. Gogotsi, A. Nikitin, H. Ye, W. Zhou, J. E. Fischer, B. Yi, H. C. Foley and M. W. Barsoum, *Nat Mater*, 2003, **2**, 591-594.
12. G. N. Yushin, E. N. Hoffman, A. Nikitin, H. Ye, M. W. Barsoum and Y. Gogotsi, *Carbon*, 2005, **43**, 2075-2082.
13. L. Radhakrishnan, J. Reboul, S. Furukawa, P. Srinivasu, S. Kitagawa and Y. Yamauchi, *Chemistry of Materials*, 2011, **23**, 1225-1231.
14. S.-M. Hong, S. W. Choi, S. H. Kim and K. B. Lee, *Carbon*, 2016, **99**, 354-360.

17. J. C. Bear, W. J. Peveler, P. D. McNaughter, I. P. Parkin, P. O'Brien and C. W. Dunnill, *Chemical Communications*, 2015, **51**, 10467-10470.
18. W. J. Chung, J. J. Griebel, E. T. Kim, H. Yoon, A. G. Simmonds, H. J. Ji, P. T. Dirlam, R. S. Glass, J. J. Wie, N. A. Nguyen, B. W. Guralnick, J. Park, A. Somogyi, P. Theato, M. E. Mackay, Y.-E. Sung, K. Char and J. Pyun, *Nature Chemistry*, 2013, **5**, 518-524.
19. A. G. Simmonds, J. J. Griebel, J. Park, K. R. Kim, W. J. Chung, V. P. Oleshko, J. Kim, E. T. Kim, R. S. Glass, C. L. Soles, Y. E. Sung, K. Char and J. Pyun, *ACS Macro Lett.*, 2014, **3**, 229-232.
20. E. T. Kim, W. J. Chung, J. Lim, P. Johe, R. S. Glass, J. Pyun and K. Char, *Polymer Chemistry*, 2014, **5**, 3617-3623.
21. T. Hasell, D. J. Parker, H. A. Jones, T. McAllister and S. M. Howdle, *Chemical Communications*, 2016, **52**, 5383-5386.
22. M. P. Crockett, A. M. Evans, M. J. H. Worthington, I. S. Albuquerque, A. D. Slattery, C. T. Gibson, J. A. Campbell, D. A. Lewis, G. J. L. Bernardes and J. M. Chalker, *Angewandte Chemie International Edition*, 2016, **55**, 1714-1718.
23. P. T. Dirlam, A. G. Simmonds, T. S. Kleine, N. A. Nguyen, L. E. Anderson, A. O. Klever, A. Florian, P. J. Costanzo, P. Theato, M. E. Mackay, R. S. Glass, K. Char and J. Pyun, *Rsc Advances*, 2015, **5**, 24718-24722.
24. J. J. Griebel, G. Li, R. S. Glass, K. Char and J. Pyun, *Journal of Polymer Science Part a-Polymer Chemistry*, 2015, **53**, 173-177.
25. J. Lim, U. Jung, W. T. Joe, E. T. Kim, J. Pyun and K. Char, *Macromolecular Rapid Communications*, 2015, **36**, 1103-1107.
26. B. Oschmann, J. Park, C. Kim, K. Char, Y.-E. Sung and R. Zentel, *Chemistry of Materials*, 2015, **27**, 7011-7017.
27. T. R. Martin, K. A. Mazzio, H. W. Hillhouse and C. K. Luscombe, *Chemical Communications*, 2015, **51**, 11244-11247.
28. M. Arslan, B. Kiskan and Y. Yagci, *Macromolecules*, 2016, **49**, 767-773.
29. D. Mhamane, W. Ramadan, M. Fawzy, A. Rana, M. Dubey, C. Rode, B. Lefez, B. Hannoyer and S. Ogale, *Green Chemistry*, 2011, **13**, 1990-1996.
30. National Institute of Standards and Technology, http://srdata.nist.gov/xps/.
31. B. J. Lindberg, K. Hamrin, G. Johansson, U. Gelius, A. Fahlman, C. Nordling and K. Siegbahn, *Physica Scripta*, 1970, **1**, 286.
32. B. B. Saha, S. Jribi, S. Koyama and I. I. El-Sharkawy, *Journal of Chemical & Engineering Data*, 2011, **56**, 1974-1981.
33. B. Crittenden, A. Patton, C. Jouin, S. Perera, S. Tennison and J. A. B. Echevarria, *Adsorption-Journal of the International Adsorption Society*, 2005, **11**, 537-541.
34. D. Lozano-Castello, M. Jorda-Beneyto, D. Cazorla-Amoros, A. Linares-Solano, J. F. Burger, H. J. M. ter Brake and H. J. Holland, *Carbon*, 2010, **48**, 123-131.
35. V. Ruiz, C. Blanco, R. Santamaria, J. M. Ramos-Fernandez, M. Martinez-Escandell, A. Sepulveda-Escribano and F. Rodriguez-Reinoso, *Carbon*, 2009, **47**, 195-200.
36. S. Basu, A. L. Khan, A. Cano-Odena, C. Liu and I. F. J. Vankelecom, *Chemical Society Reviews*, 2010, **39**, 750-768.
37. K. K. Sirkar, *Chemical Engineering Communications*, 1997, **157**, 145-184.
38. Y. Zhang, J. Sunarso, S. Liu and R. Wang, *International Journal of Greenhouse Gas Control*, 2013, **12**, 84-107.
39. R. W. Baker, *Ind. Eng. Chem. Res.*, 2002, **41**, 1393-1411.

Nakanishi, *Chemistry of Materials*, 2015, **27**, 4705-4712.
42. W. Kicinski, M. Szala and M. Bystrzejewski, *Carbon*, 2014, **68**, 1-32.
43. M. S. Shafeeyan, W. M. A. W. Daud, A. Houshmand and A. Shamiri, *Journal of Analytical and Applied Pyrolysis*, 2010, **89**, 143-151.
44. M. Sevilla and A. B. Fuertes, *Microporous Mesoporous Mat.*, 2012, **158**, 318-323.
45. Y. D. Xia, Y. Q. Zhu and Y. Tang, *Carbon*, 2012, **50**, 5543-5553.
46. H. A. Patel, F. Karadas, J. Byun, J. Park, E. Deniz, A. Canlier, Y. Jung, M. Atilhan and C. T. Yavuz, *Advanced Functional Materials*, 2013, **23**, 2270-2276.
47. H. A. Patel, M. S. Yavuz and C. T. Yavuz, *Rsc Advances*, 2014, **4**, 24320-24323.
48. D. M. D'Alessandro, B. Smit and J. R. Long, *Angewandte Chemie-International Edition*, 2010, **49**, 6058-6082.
49. M. B. Shiflett and H. C. Foley, *Science*, 1999, **285**, 1902-1905.

Tables

Table 1: Synthetic quantities of each reagent added for various compositions of S-DIB copolymer, and quantitative ratios of sulfur : carbon obtained by quantitative XPS:

Sample / wt.% (of DIB)	1,3-diisopropenylbenzene / ml (mmol)	Sulfur / g (mmol)	Sulfur / % conc.	Carbon / % conc.
5	0.114, 0.665	2, 7.81	9.5	90.5
10	0.240, 1.40	2, 7.81	11.1	88.9
20	0.541, 3.16	2, 7.81	14.1	85.9
40	1.44, 8.40	2, 7.81	11.8	88.2
50	2.16, 12.6	2, 7.81	7.4	92.6

Figures

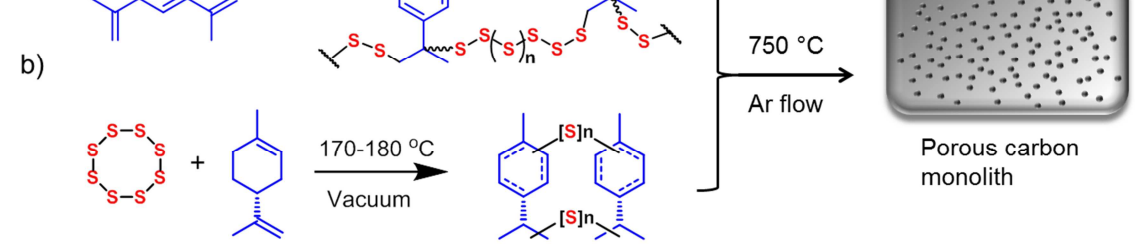

Scheme 1. a) Sulfur-diisopropenyl benzene (S-DIB) copolymer synthesis, b) sulfur-limonene (S-Lim) copolymer synthesis, and c) subsequent carbonisation method.

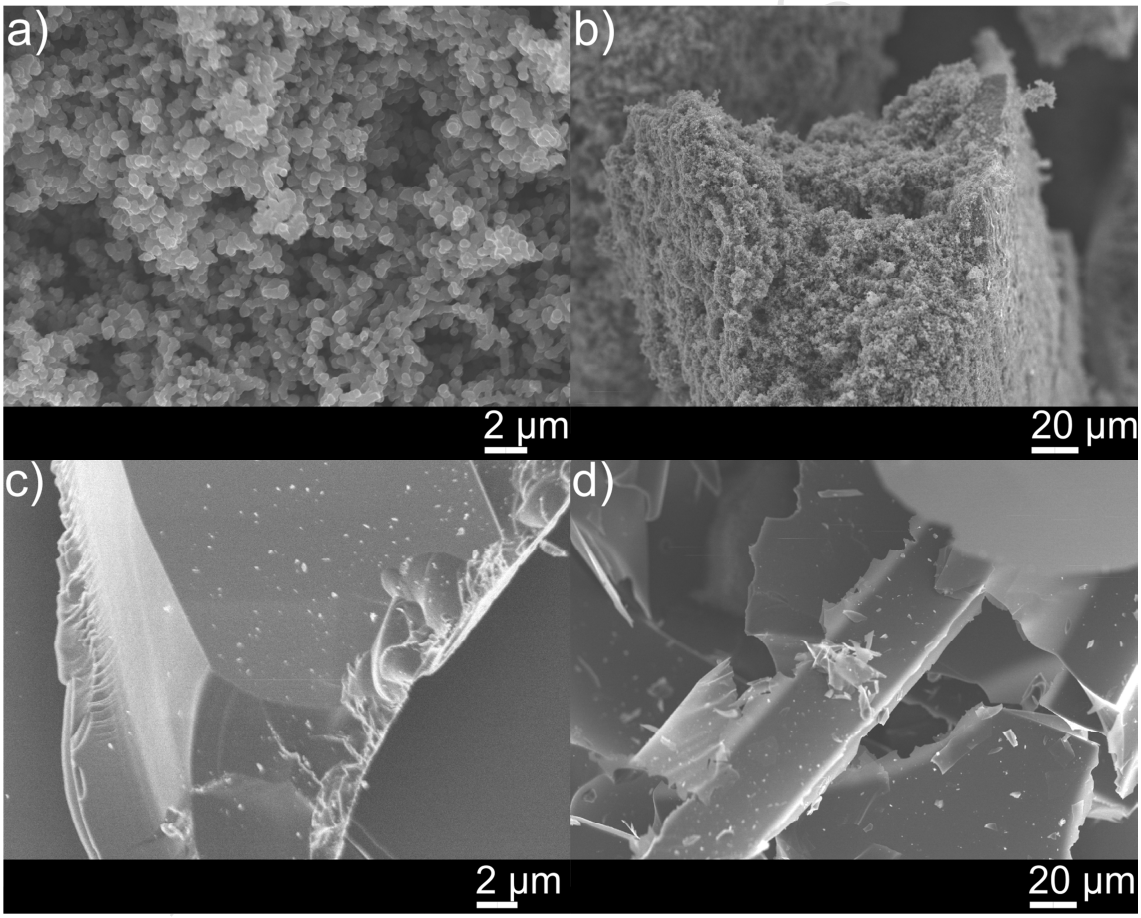

Figure 1. SEM images of: a) and b) high sulfur (90 wt. % S) polymer showing the porous microstructure of the monolith and c) and d) as the smooth, low sulfur (50 wt. % S) polymer sample, showing the smooth architecture.

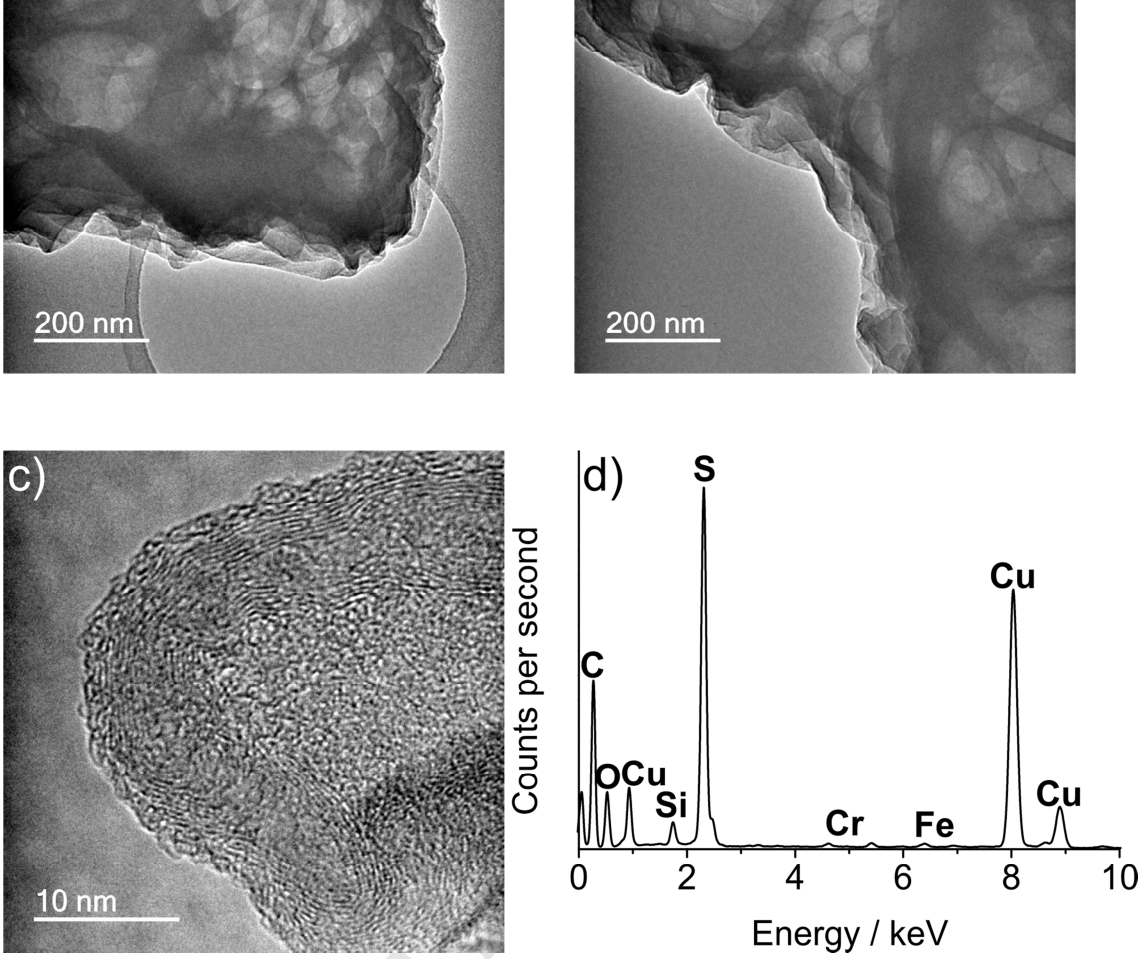

Figure 2. TEM images of a carbonised sample of S-DIB (40 wt% DIB). Images a) and b) show the internal voids in the structure, from removal of sulfur during carbonisation. HRTEM, c), reveals some degree of local order and crystallinity in the carbonised material. EDS analysis, d), indicates the presence of carbon and sulfur. It should be noted that copper emanates from the copper sample grid and chromium and iron emanate from the steel sample holder.

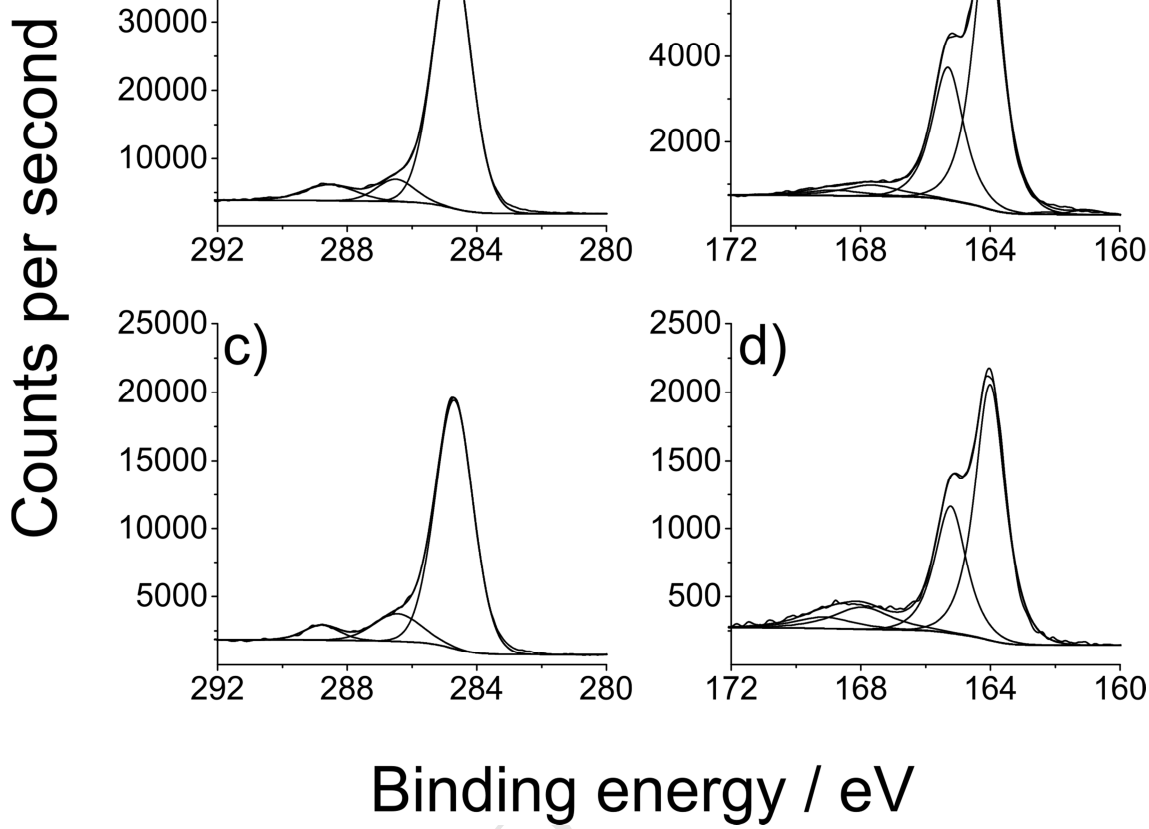

Figure 3. High resolution XPS scans of C1s and S2p of 10 wt. % and 50 wt. % DIB content sulfur polymers after carbonisation: a) 10 wt % C1s, b) 10 wt. % S2p, c) 50 wt. % C1s and d) 50 wt. % S2p.

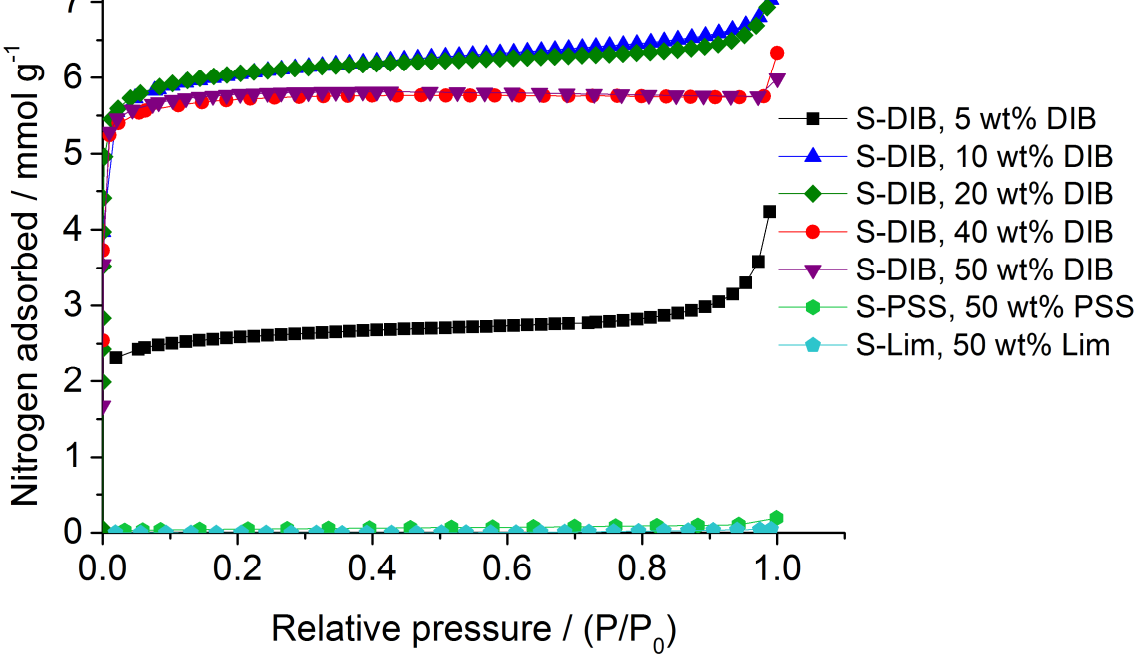

Figure 4. Nitrogen adsorption isotherms (at 77.3 k, 1 bar) of carbonised samples of S-DIB polymers, as well as S-limonene copolymer (S-Lim) and a sulfur-poly(4-styrenesulfonate) mixture (S-PSS).

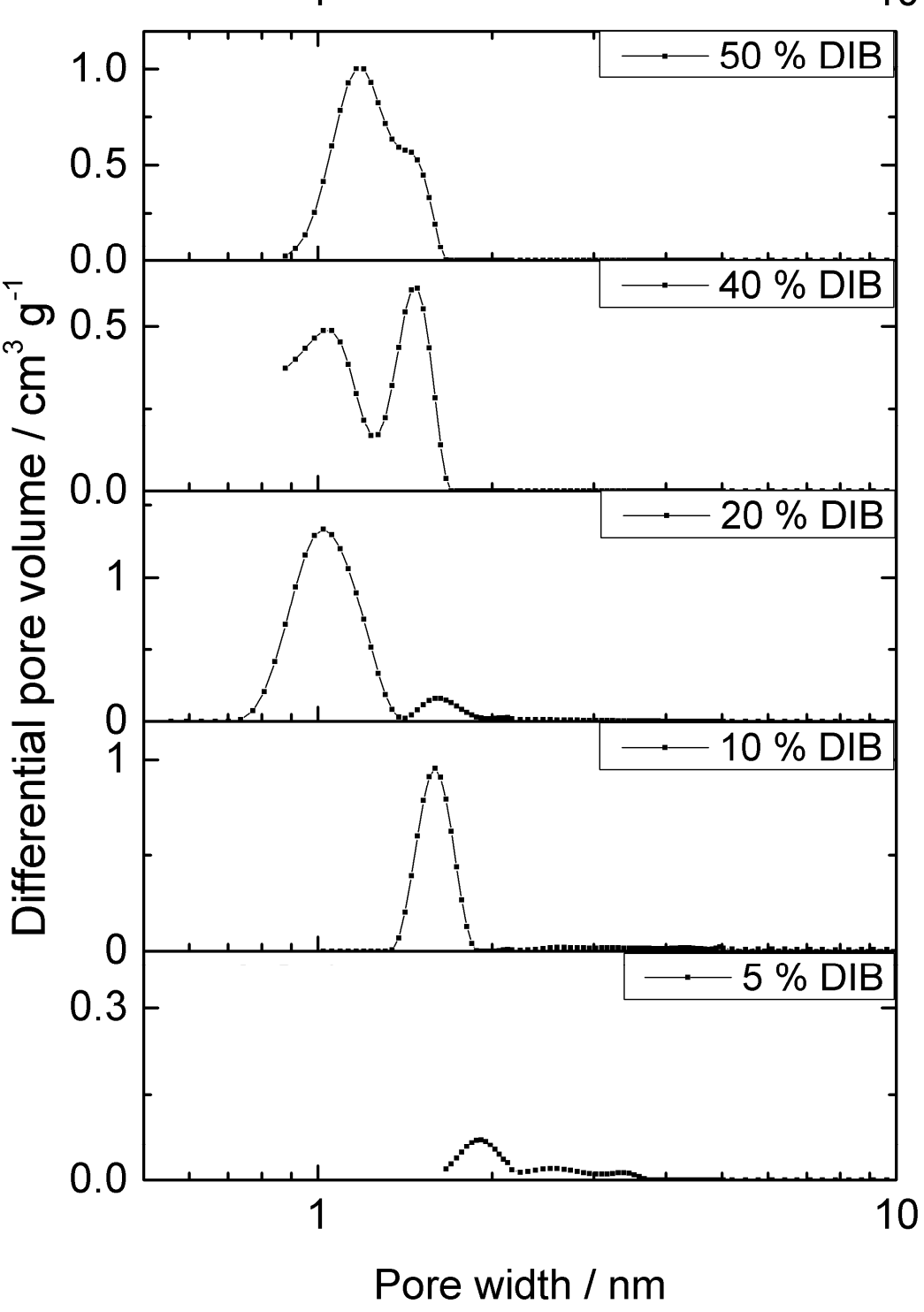

Figure 5. (b) NL-DFT pore size distribution, calculated from the nitrogen isotherms, for a series of carbonised S-DIB copolymers.

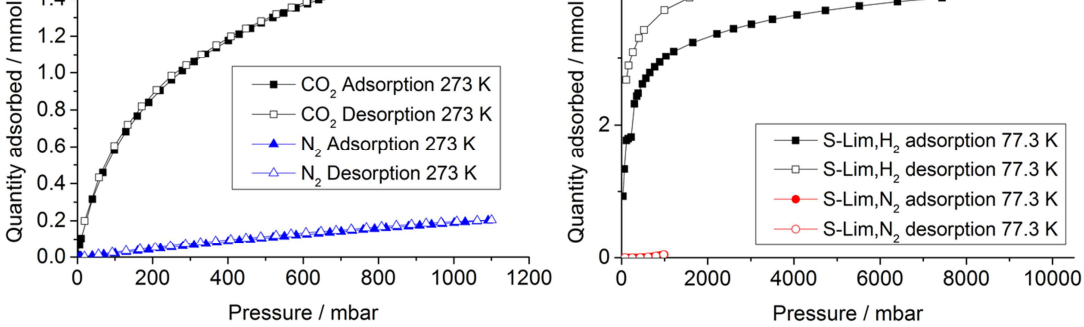

Figure 6. a) Adsorption isotherms (solid symbols) and desorption isotherms (open symbols) for carbon dioxide and nitrogen on carbonised S-Lim (50 wt% limonene), up to 1 bar pressure and at 273 K. b) Adsorption isotherms (solid symbols) and desorption isotherms (open symbols) for hydrogen and nitrogen on carbonised S-Lim (50 wt% limonene), up to 10 bar pressure and at 77.3 K.

Supplementary information:

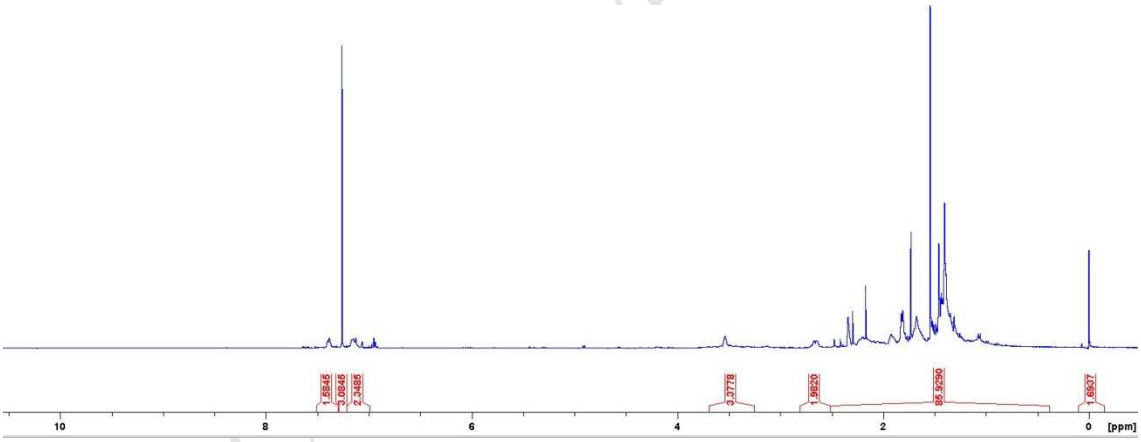

Figure S1. ^{1}H NMR spectrum of the sulfur-limonene polysulfide produced.

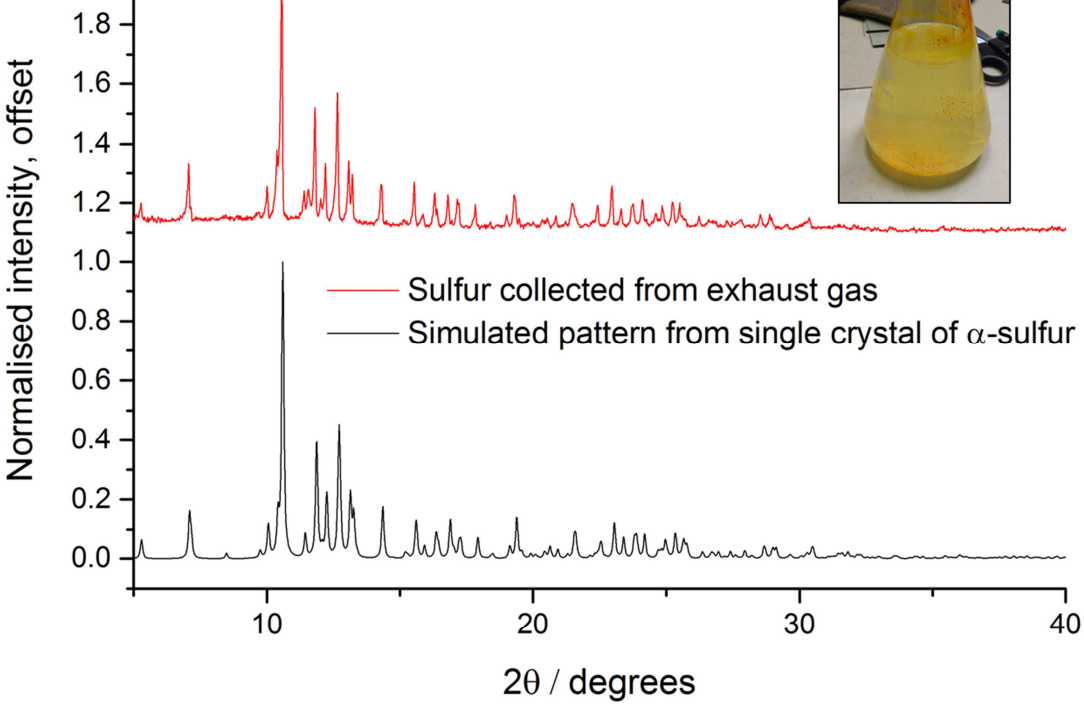

Figure S2. Powder XRD of the yellow precipitated powder collected from water through which the exhaust gas was bubbled (inset). As can be seen, the experimental pattern matches the common α form of elemental sulfur.

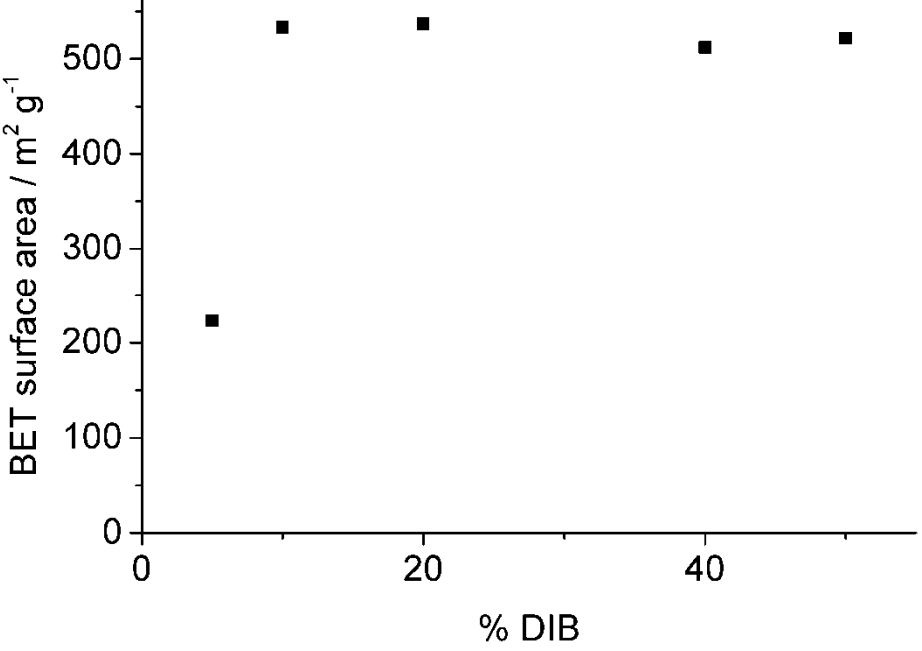

Figure S3. Apparent BET surface area as a function of initial DIB content in carbonised S-DIB copolymers.

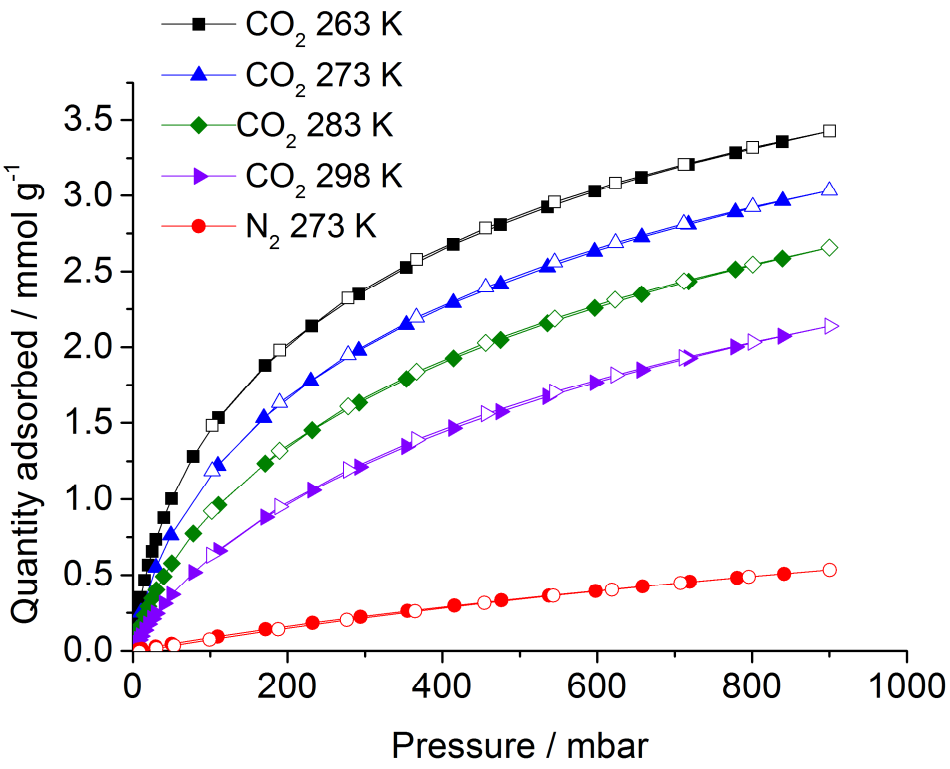

K is included for comparison.

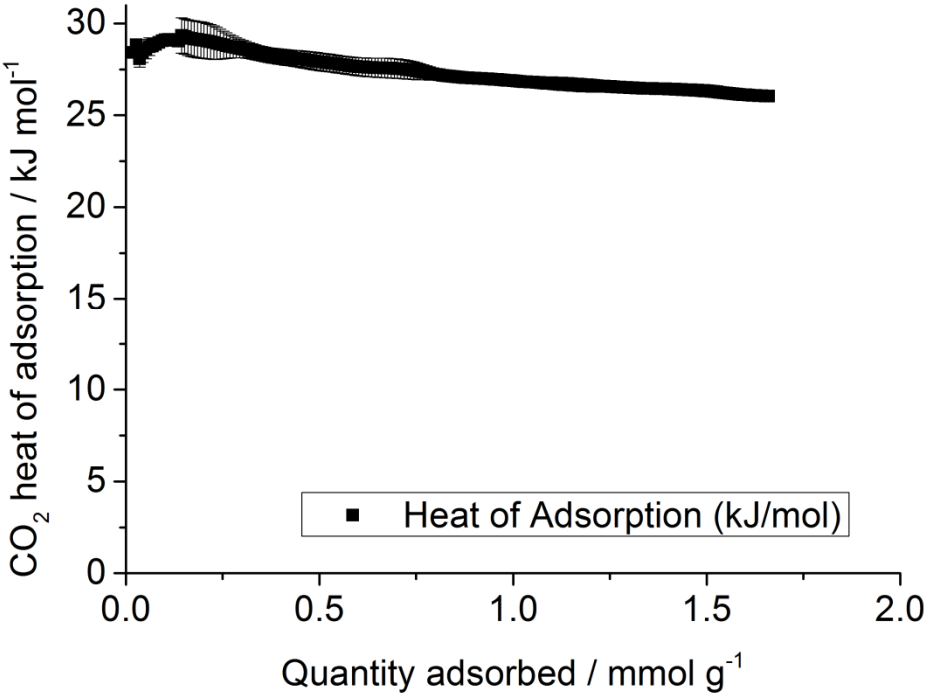

Figure S5. Isosteric heat (*Q*st/ kJ mol^{-1}) of adsorption for CO_2 as a function of the amount adsorbed (mmol g^{-1}) for the temperature range 263–298 K, determined using the standard calculation routines in the Data-master offline data reduction software (Micromeritics), for 10 wt. % DIB carbonised S-DIB.

Figure S6. Photograph of a large sulfur-carbon monolith synthesised from annealing 20 g of ground 50 wt. % DIB polymer at 750 °C for 1 hour under N_2. For scale, a UK 50 pence piece is added.

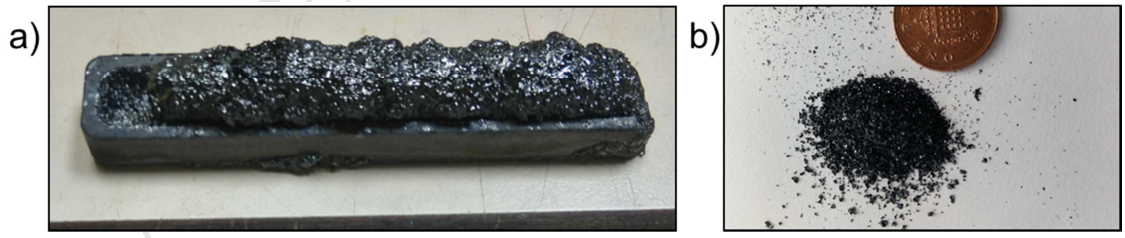

Figure S7. a) Photograph of a sulfur-carbon monolith synthesised from annealing 4 g of 50 wt. % Limonene polymer at 750 °C for 1 hour under N_2. b) powdered form of the carbonised S-limonene polymer after breaking it up for sorption analysis.

- Produces sulfur-doped microporous and gas selective monoliths